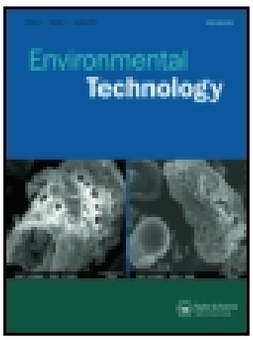

Environmental Technology

ISSN: 0959-3330 (Print) 1479-487X (Online) Journal homepage: http://www.tandfonline.com/loi/tent20

# Green synthesis of nano-zero-valent iron from Nettle and Thyme leaf extracts and their application for the removal of cephalexin antibiotic from aqueous solutions

Mostafa Leili, Mehdi Fazlzadeh & Amit Bhatnagar

**To cite this article:** Mostafa Leili, Mehdi Fazlzadeh & Amit Bhatnagar (2017): Green synthesis of nano-zero-valent iron from Nettle and Thyme leaf extracts and their application for the removal of cephalexin antibiotic from aqueous solutions, Environmental Technology, DOI: 10.1080/09593330.2017.1323956

**To link to this article:** http://dx.doi.org/10.1080/09593330.2017.1323956

Accepted author version posted online: 26 Apr 2017.
Published online: 12 May 2017.

ENVIRONMENTAL TECHNOLOGY, 2017
https://doi.org/10.1080/09593330.2017.1323956

Taylor & Francis
Taylor & Francis Group



# Green synthesis of nano-zero-valent iron from Nettle and Thyme leaf extracts and their application for the removal of cephalexin antibiotic from aqueous solutions

Mostafa Leili [a], Mehdi Fazlzadeh [b] and Amit Bhatnagar [c]

[a]Department of Environmental Health Engineering, School of Public Health and Research Center for Health Sciences, Hamadan University of Medical Sciences, Hamadan, Iran; [b]Department of Environmental Health Engineering, School of Public Health, Ardabil University of Medical Sciences, Ardabil, Iran; [c]Department of Environmental Science, University of Eastern Finland, Kuopio, Finland

**ABSTRACT**

In this study, the removal of cephalexin (CEX) antibiotic from aqueous solution was examined using a novel green adsorbent without employing any toxic chemicals or capping agents. Nettle and Thyme extracts were used to synthesize novel nano-zero-valent iron (NNZVI and TNZVI) for the adsorption of CEX. The nature and morphology of synthesized adsorbent were characterized by Transmission electron microscopy, scanning electron microscope, X-ray diffraction and Fourier transform infrared spectroscopy spectroscopy. Batch experiments were performed to study the influence of various experimental parameters such as contact time, initial concentration of the CEX, solution pH and adsorbent dosage. The adsorption isotherms of CEX by NNZVI and TNZVI were found to fit well with Freundlich and Langmuir models, respectively. The maximum adsorption capacity of CEX onto NNZVI and TNZVI were observed as 1667 and 1428 mg/g, respectively, based on the Langmuir model. The adsorption trend followed the pseudo-first-order kinetics model and equilibrium could be established in about two hours for both adsorbents. The developed nanoparticles in this study have considerable potential for the removal of CEX and could be considered as a promising adsorbent for the removal of other antibiotics also from aqueous solutions.

**ARTICLE HISTORY**
Received 15 December 2016
Accepted 21 April 2017

**KEYWORDS**
Green synthesis method; cephalexin; Nettle and Thyme nanoparticles; adsorption

## 1. Introduction

Over the past few decades, occurrence of organic micropollutants such as pharmaceuticals in the aquatic ecosystems has been considered as a major environmental and health issue globally [1,2]. Pharmaceuticals have become chemicals of emerging concern to the public because of their potential to reach drinking water. Cephalexin (CEX) is one of the main antibiotics of the cephalosporin family [3,4]. It is commonly being used for the treatment of many infectious diseases including infections of respiratory tract, ear, skin, soft tissue, skeletal and urinary tract [3,5]. Similar to other antibiotics, CEX may pass through the human and animal bodies as an un-metabolized compound [3,6]. Due to the stability of the antibiotic in the environments, high levels of antibiotics may sometimes occur in wastewater treatment plants and also in water distribution systems [7,8]. Sources of antibiotics in the environment include sanitary wastewater, effluents of pharmaceutical industries, animal wastes and also solid waste leachates which may occur in various levels ranging from ng/L to mg/L [1,9–11]. Long-term exposure to antibiotics may cause acute disorders in human and pose serious threats to the environment [3,12]. Furthermore, antibiotics in natural water may promote antibiotic-resistant microorganisms [13,14].

Therefore, it is essential to remove antibiotics from wastewater before being discharged into the environment or surrounding water bodies [3,6]. Various methods like biological technique [15,16], catalytic ozonation [17,18], adsorption on carbon nanotubes [19,20] and on iron nanoparticles [21], membrane separation [22], sonochemical process [13], etc. have been used to remove CEX. However, these methods have some limitations. For example, although biological methods are environmentally friendly [23], they have some inhibitory effects on microbial metabolism, particularly at high concentrations, because of low biodegradability resulted from the presence of stable rings of nephthol [15,24,25]. Also, chemical techniques impose some operational costs such as electric power and materials shipment; some chemicals (e.g. ozone), which are used in advanced oxidation processes, are highly corrosive and toxic [26–30]. Membrane processes also do not have desirable effectiveness in the removal of antibiotics because of membrane fouling issues and vulnerability of the membranes to organic solvents of effluents

CONTACT Mehdi Fazlzadeh m.fazlzadeh@gmail.com School of Public Health, Ardabil University of Medical Sciences, Ardabil, Iran

[22,31]. Thus, these disadvantages could limit the applications of these processes.

Adsorption, an effective separation process, has attracted considerable attention compared to other techniques because of the advantages in terms of cost, reusability of effluents, ease of operation, flexibility and simplicity of design and the absence of reaction with pollutants or toxic compounds [3,32–34]. Other advantages such as production of a high-quality effluent and absence of formation of free radicals and hazardous materials have also been reported by this method [6,35]. Accordingly, a variety of natural and synthetic materials including activated carbon [6,9], clay [36], zeolite [5], bentonite [37] and various nanoparticle [19,21,38] have been tested for the adsorption of CEX.

Nanoparticles have been found to be efficient materials for CEX removal, which have the capability to be used as adsorbent, photo-catalyst, membrane materials and disinfectants. Nanoparticles are produced by physical and chemical methods [39–41]. Recently, the green synthesis of nanoparticles is in focus as a cost-effective and environmentally friendly method alternative to physical and chemical methods [42]. Production of nanoparticles from the extracts of plants is cost-effective and the products have no hazardous effects on the environment and can also be produced on large scales. The precursors of nanoparticles in this method are polyphenols and caffeine existing in plant extracts, which are nontoxic and biodegradable in the environment [43,44]. They function as reducing as well as stabilizing agents [42,45].

Thus, in the present study, Nettle and Thyme as two abundant local plants (in Ardabil province, northwestern Iran) with therapeutic potential were selected to synthesize zero-valent iron nanoparticles (NZVI) from these plants by a green synthesis method. The nature and morphology of the synthesized adsorbent were characterized by Transmission electron microscopy (TEM), scanning electron microscope (SEM), X-ray diffraction (XRD) and Fourier transform infrared spectroscopy (FTIR) spectroscopy. The potential of synthesized nanoparticles for the adsorption of CEX was subsequently investigated. Batch experiments were performed to study the influence of various experimental parameters such as contact time, initial concentration of the CEX, solution pH and adsorbent dosage.

## 2. Materials and methods

### 2.1. Materials

CEX ($C_{16}H_{17}N_3O_4S$; MW = 347.39 g/mol) was purchased from Sina Daru Co. (Iran) and used without any further treatment. All the primary chemicals used in this study were of analytical grade and obtained from Merck, Germany. All solutions were made with double distilled water. The pH of the solutions was adjusted with hydrochloric acid (HCl) and sodium hydroxide (NaOH) (0.1 N). The stock solution of CEX was prepared by dissolving the appropriate amount of powdered CEX of purity 97% in the solution containing 950 mL of double distilled and 50 mL of 1 M NaOH and kept in a glass container at room temperature. Required working concentrations of CEX standards were instantaneously prepared through the appropriate dilution of this stock solution for each experiment.

### 2.2. Green synthesis of NZVI from Nettle and Thyme leaf extracts

Dried leaves of Nettle and Thyme were purchased from the market and then washed several times with double deionized water to remove any dust and dried at room temperature. After that, the extracts of Nettle and Thyme were prepared by boiling 60 g/L of the leaves of these plants at 80°C for 1 h. After 1 h, the extracts of Nettle and Thyme were filtered by a vacuum pump. Then, 0.1 M $FeCl_2.4H_2O$ solution was added to 60 g/L of Nettle and Thyme extracts in the ratio of 2:3. Solution pH was adjusted at 6 by adding 1M NaOH [44]. At this time, the Nettle and Thyme zero-valent iron nanoparticles appeared as black colored precipitates. The formed nanoparticles were separated by evaporation on a hot plate surface and collected by washing several times with deionized water and placed in nitrogen gas to avoid oxidation [46,47] and named as NNZVI and TNZVI in the study.

### 2.3. Analysis of CEX

A colorimetric method was used to analyze the CEX concentration of the samples. CEX was measured at the wavelength of 276 nm [3,6] using a double beam spectrophotometer (Model lambda 25- Perkin Elmer Company).

### 2.4. Zero point of charge determination

The pH at the zero point of charge ($pH_{ZPC}$) has been used to characterize the electrochemical properties of adsorbents. To perform this, 0.01 M NaCl was used as an electrolyte by adding 0.1 N NaOH or 0.1 N HCl solutions. To determine the $pH_{ZPC}$ of each synthesized nanoparticle, 50 mL of the prepared electrolyte solution was introduced into eight beakers to adjust their pH at the required values of 2–12. Subsequently, 0.1 g of both

NNZVI and TNZVI were added into each beaker and were shaken for 24 h. After this period of agitation, the solution was filtered and the final pH of the filtrate was measured. At the last step, ZPC of the nanoparticles was determined from the intersection of plotting the initial pH versus the final pH [48].

### 2.5. Adsorption experiments

The adsorption of CEX by NNZVI and TNZVI was conducted in batch mode. For each experiment, 250 mL of the CEX solution of desired concentration was added into Erlenmeyer flasks. The desired pH for each experiment was adjusted using 0.1 N HCl and NaOH. Then, the predetermined dose of NNZVI and TNZVI was added into the Erlenmeyer flask and the mixture was agitated at regulated speed by a shaker. After the desired contact time, the samples were filtered through Whatman filter paper (0.2 µm) and then centrifuged (5810 R, Eppendorf Biotech Company). The CEX concentration was analyzed by spectrophotometer to determine the residual CEX concentration.

The main process parameters studied were solution pH (initial pH 2, 4, 6, 7, 9, 11), initial CEX concentrations (25, 50, 100, 150, 200 and 300 mg/L), adsorbent doses (0.05, 0.1, 0.4, 0.6, 0.8 and 1 g/L) and contact time (1, 5, 10, 15, 20, 25, 30, 45, 60 and 70 min). All the experiments were conducted at room temperature in triplicate to ensure the reproducibility of the results with a standard deviation less than 10%.

For kinetics studies, 0.1 g/L of the adsorbent was contacted with 250 mL of CEX solutions with the initial concentrations of 25, 50 and 100 mg/L of CEX. In all kinetic experiments, the pH of the solution was kept at optimum (≈2), which was predetermined by studying the pH effect. For equilibrium studies, various concentrations of CEX ranging from 10 to 700 mg/L were chosen and a fixed adsorbent dose of 0.1 g/L was added. The flasks were capped and the contents were stirred for 2 h and filtered afterwards.

The CEX adsorption capacities at equilibrium, $q_e$ (mg CEX/g adsorbents), were determined using Equation (1):

$$q_e = \frac{(C_0 - C_e) \times V}{m}, \quad (1)$$

where $C_0$ and $C_e$ are initial and final concentrations of CEX (mg/L), respectively, $V$ is the volume of solution ($L$) and m is the mass ($g$) of the adsorbent as dry weight.

The kinetics of CEX adsorption onto NNZVI and TNZVI were analyzed by fitting data from the experiment of this step with the pseudo-first-order and pseudo-second-order models as shown in Table 1. In this table, $k_1$ and $k_2$ are constants of adsorption rate, $q_t$ is adsorption capacity at time $t$ and $q_e$ is adsorption capacity at equilibrium, respectively. Regarding that adsorption isotherm analysis is crucial to understand the interaction between an adsorbate and the adsorbent or to describe the nature of the adsorption [5,9,49]; thus, to provide quantitative information, these data were fitted by the Langmuir and Freundlich isotherm models by using the equations presented in Table 1. The $q_m$ parameter is the maximum adsorption capacity (mg/g), $b$ is a constant related to the energy of adsorption (L/g), $K_F$ is a constant related to the adsorption capacity (mg/g) and can be defined as the distribution coefficient, which with the increases of $K_F$ values, the adsorption capacity of the adsorbent also increased.

**Table 1.** The name and equations of the studied isotherm and kinetic models.

| Model types | Name | Equation | Ref. |
|---|---|---|---|
| Isotherm models | Langmuir | $\frac{C_e}{q_e} = \frac{C_e}{q_{max}} + \frac{1}{q_{max} b}$ | [39] |
| | Freundlich | $\log q_e = \log k_f + \frac{1}{n} \log C_e$ | [39] |
| Kinetic models | Pseudo-second-order model | $q_t = \frac{q_e^2 k_2 t}{q_e k_2 t + 1}$ | [40] |
| | Pseudo-first-order model | $q_t = q_e - \exp(\ln q_e - k_1 t)$ | [41] |

To evaluate the goodness of fit of a kinetic and an isotherm model and to describe the sorption phenomena, the predicted versus experimental values were evaluated by comparing chi-square statistic ($\chi^2$), which has extensively been used as an appropriate statistic means for comparing the models with two parameters [50]:

$$\chi^2 = \frac{(q_{e,exp} - q_{e,cal})^2}{q_{e,cal}}, \quad (2)$$

where $q_{e,exp}$ and $q_{e,cal}$ (mg/g) are the experimental and model estimated equilibrium capacity data, respectively. The small and large values of $\chi^2$ means that data calculated from the model are similar to experimental values or different, respectively.

### 2.6. Characterization of surface properties and chemical composition

A SEM equipped with an energy-dispersive X-ray microanalysis (LEO-1430 VP) was used to determine the surface morphology and the porous structure of the NNZVI and TNZVI. The surface functional groups of adsorbents were determined using FTIR at wave numbers ranging from 400 to 4000 $cm^{-1}$. To explore the structure of the material, XRD patterns of synthesized NZVI before adsorption were studied using a Philips X'Pert Pro instrument (Netherlands) within the $2\theta$ range of 10–90°. The X-ray source was radioactive Cu–

Kα (λ = 154 nm). TEM was used to get particle sizes using a JEOL JEM 1200 EX Mk 2 TEM, operating at 120 keV. The nanoparticle samples were sonicated in methanol with analytical grade for 30 s and then mounted on 200-mesh holey carbon-coated copper grids.

## 3. Results and discussion

### 3.1. Characterization of synthesized NZVI

Figure 1(a, b) show FTIR spectra for NNZVI and TNZVI, respectively, before and after adsorption with CEX. As seen, an absorption band is observed at wave numbers between 3000 and 4000 $cm^{-1}$ for both NNZVI and TNZVI (with maximums of 3405 and 3398 $cm^{-1}$ for NNZVI and TNZVI, respectively), with this broad peak around 3400 $cm^{-1}$ indicating the O–H bond vibrations on the adsorbent surface [51]. The change or appearance of the peak near 2933 and 2944 $cm^{-1}$ suggests the involvement of C–H ($sp^3$ hybridized) and O–H (of acid origin) group of leaf extract in particle formation [52]. The O-H deformation vibration to $C=O$ asymmetric stretching vibration was observed near 1621 $cm^{-1}$ (of acids) for both adsorbents [5,53]. The peaks of 1384 $cm^{-1}$ (and 1430 $cm^{-1}$) and 1423 $cm^{-1}$ for NNZVI and TNZVI correspond to the stretching bands of $CH_3$ bend and C–C stretch, which in turn demonstrate that oxygen was functioning to stretch acidic carboxylic groups and that carboxylate groups were available on the adsorbents' nanosphere surface [54]. The peaks at ~1117 $cm^{-1}$ for both NNZVI and TNZVI may also correspond to C–CO–C stretching of carbonyl compounds [55,56]. The remaining absorption wave number from 615 to 605 $cm^{-1}$ for NZVI was possibly due to aliphatic C–H stretch [57]. Furthermore, as clearly seen in Figure 1(a, b), the new peaks appear in synthesized nanoparticles at wavenumbers of 1621 and 613 $cm^{-1}$ for NNZVI, and at wavenumbers of 3398 $cm^{-1}$ for TNZVI which could be attributed to compounds such as alkenes, alkanes and polyphenols. After the adsorption of CEX onto NNZVI and TNZVI, the bands declined and new bands were evident at 3391 and 3381 $cm^{-1}$, respectively. The new bands indicated the presence of the corresponding organic functional groups on the NZVI surface, which should be related to the reduction products of CEX. For example, it should be attributed to possible carboxylic acid functional groups. Finally, the FTIR spectrum of after CEX adsorption to NZVI shows lower transmission percentages at all observed bands compared to fresh ones, implies that adsorption capacity of synthesized adsorbents did not significantly changed.

The surface morphology of NNZVI and TNZVI has been shown in Figure 2(a–f), indicating mainly mesoporous structures of synthesized NZVI. These structures were not observed in the fresh Nettle and Thyme (Figure 2(a, b)), but as can be seen in Figure 2(b, e), NNZVI has an irregular morphology and there are many naometer-scale spherical aggregates clearly showing a smooth surface with scattered cavities and bumps. The presence of these bumps with various sizes on the surface of the adsorbents, in turn, makes it a well-supported material mainly due to the increases of the chance of CEX molecules' trapping and subsequent adsorption onto the surface of the adsorbent. Figure 2(c, f) show the SEM image of CEX-loaded NNZVI and TNZVI. As can clearly be seen, these cavities were filled with adsorbed CEX. However, the specific base materials and their strength and texture composition may be responsible for the difference in surface morphology of NNZVI and TNZVI.

TEM images and XRD patterns of NZVI have been shown in Figure 3. As shown in Figure 3(a–b), the synthesized nanoparticles tend to form irregular clusters but also demonstrate some dispersion, and the analysis confirmed that metallic iron particles were produced with particle size ranging roughly between 20 and 80 nm. The XRD patterns of NZVI were characterized after repeated sample washing with ethanol to reduce the amount of NaCl crystals but, as shown in Figure 3(c), some peaks were observed which are related to NaCl crystals. The XRD patterns of both synthesized NZVI before reaction with CEX (Figure 3(c)) have characteristic peaks at $2\theta = 11.8°$, ≈17°, 20.35°, ≈29°, ≈35°, ≈38°, ≈40°, 44.9°, 52°, 56°, 62° mainly corresponding to zero-valent iron (α-Fe), maghemite (γ-$Fe_2O_3$), magnetite ($Fe_3O_4$) and iron oxohydroxides, in addition to NaCl [42,45] due to the fact that the Nettle and Thyme were partly oxidized during the synthesis. The organic materials adsorbed from plant extract as capping/stabilizing agents can be seen as a broad hump shoulder peak at $2\theta = 25°$.

### 3.2. Adsorption kinetics

The effect of contact time for the adsorption process was carried out to determine the equilibrium point for a period of 0–40 min for NNZVI (Figure 4(a)) and 0–70 min for TNZVI (Figure 4(b)) at initial CEX concentrations of 25, 50 and 100 mg/L. But to ensure equilibrium, the samples were left for 2 h in equilibrium isotherm experiments. The other parameters of the study were kept constant in the optimum values, which were previously determined. The amount of adsorbed adsorbate was raised with increasing contact time until equilibrium and the curves for CEX adsorption with respect to time were single smooth and finally led to saturation

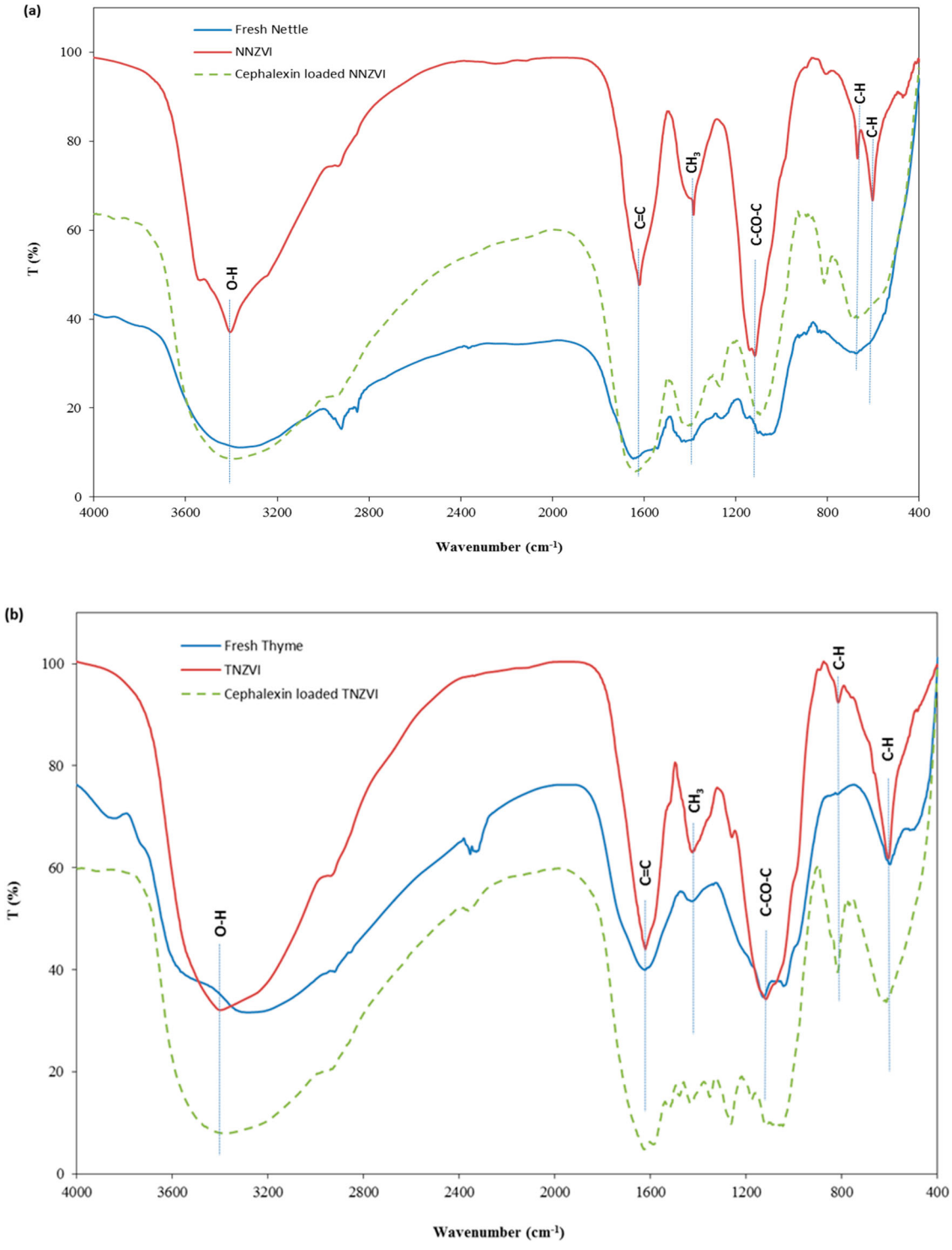


**Figure 1.** FTIR spectra of (a) NNZVI and (b) TNZVI.

conditions. In addition, it was found for all sets of the experiments that the adsorption was rapid in the initial stages of the process mainly because of higher driving forces resulting from largest amount of CEX [58] and later on became slow, and finally the systems reached equilibrium in about 50 min for both adsorbents; however, a further increase in the contact time had a negligible effect on the efficiency of the adsorption process.

It is also clear from Figure 4(a, b) that the necessary time to reach equilibrium is variable and depends on the initial concentration of the CEX, which increased with an increase in initial CEX concentration. For example, it was found to be about 30 min and 45 min

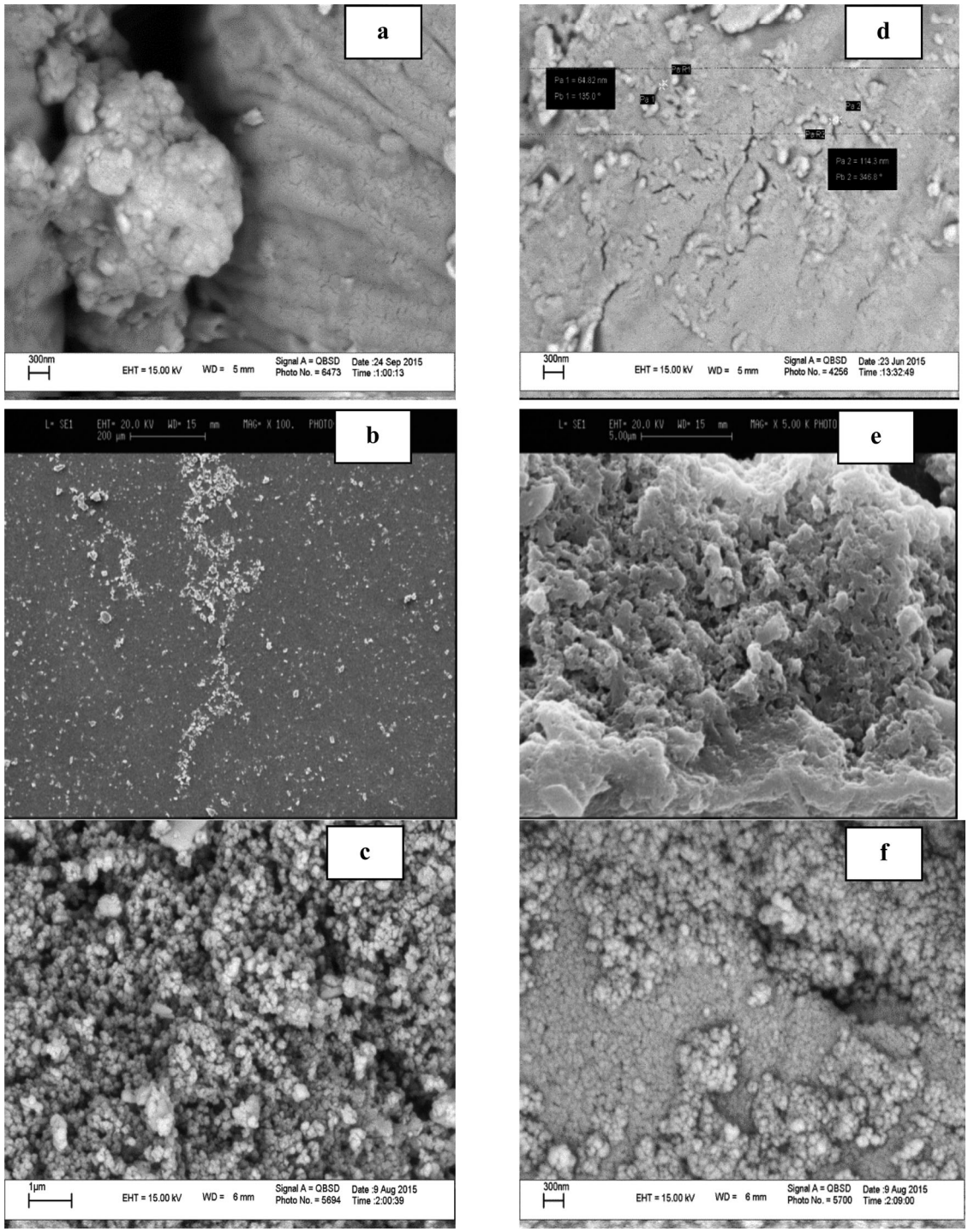


**Figure 2.** SEM micrograph of (a) fresh (raw) Nettle, (b) NNZVI, (c) CEX-loaded NNZVI, (d) fresh (raw) Thyme, (e) TNZVI and (f) CEX-loaded TNZVI.

for initial concentration of 25 and 50 mg/L for NNZVI and TNZVI, respectively. Furthermore, as the synthesized NZVI are prone to agglomeration, these agglomerates can provide an ideal place for CEX removal from aqueous phase. The agglomerates also cause the CEX to attach in multilayer behavior to the spaces between nanoparticles and longer time to be available for nanoparticles' penetration into smaller pores and more internal adsorption sites [59]. The mechanism is more predominant at higher CEX concentrations. The increase of $q_t$ with the increase of contact time confirms this behavior of synthesized NZVI.

As presented in Table 2, the adsorption of CEX onto the synthesized NZVI is well described with the

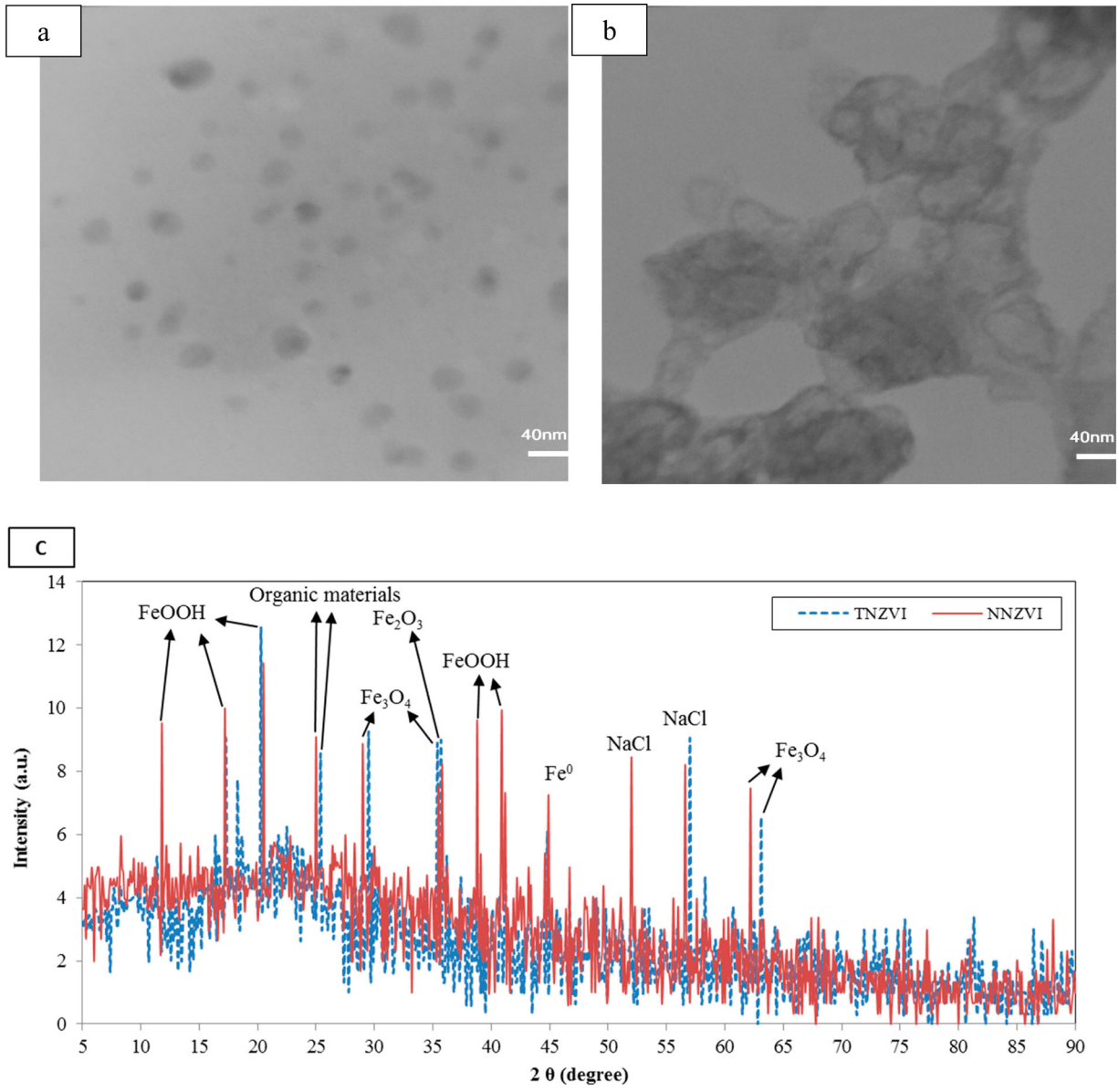


**Figure 3.** Representative TEM images of the synthesized (a) NNZVI and (b) TNZVI and (c) XRD patterns of iron nano-impregnated particles.

Lagergren's pseudo-first-order kinetic model having the highest values of the coefficient of determination ($R^2$) and lowest $\chi^2$ for all studied concentrations. Available literature on the adsorption of CEX onto NZVI is limited. However, Siqing Xia et al. [60] reported the better fitness of the adsorption of chloramphenicol onto nano scale zero-valent iron particles to the Lagergren's pseudo-first-order model. In another study, conducted by Xiulan Weng et al. [61], it was also shown that degradation of malachite with the iron-based nanoparticles synthesized from green tea extracts followed the pseudo-first-order model.

As shown in Table 2, an increase in initial CEX concentration led to decrease in the pseudo-first-order model rate constant values from 0.119 to 0.079 $k^{-1}$ and from 0.070 to 0.061 $k^{-1}$ for NNZVI and TNZVI, respectively, which are in agreement with the study of Benguella and Benaissa [62]. This downward trend in rate constant with the increase of CEX concentration implies that there has not been any limitation to adsorption sites and that the adsorption is limited only by the concentration of CEX and hence by the mass transfer rate [51]. It could also be said that, the more the initial CEX concentration, the higher would be the adsorption capacity of the adsorbents, but the adsorption efficiency of the adsorbent is inversely related to the initial CEX concentration at a fixed adsorbent dosage [49,63], Accordingly, it could be said that the increase of initial CEX

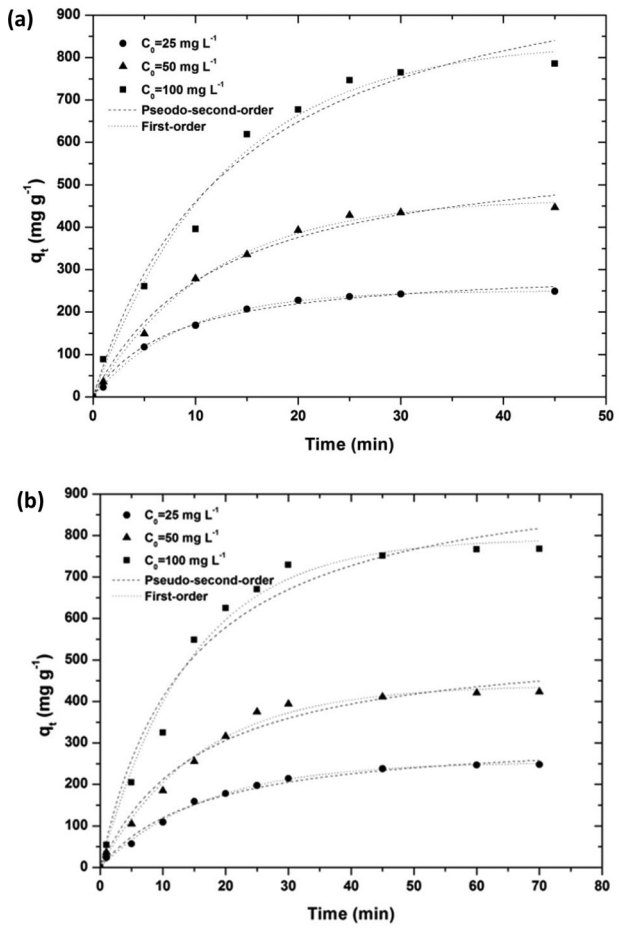


**Figure 4.** Effect of contact time on CEX adsorption onto (a) NNZVI and (b) TNZVI (adsorbent concentration = 0.1 g/L, pH = 2, shaking speed = 200 rpm at room temperature).

concentration can improve the mass transfer rate through the increase of driving force [47]. This phenomenon is further discussed in Section 3.3.

Accordingly, the availability of active adsorption sites on the surface of NNZVI and TNZVI has more influence than CEX concentration in the solution on its removal [6]. It also implies that the electrostatic attraction among carboxyl anions (as shown in Section 3.1) in the structure of antibiotic molecules and positively charged functional groups (adsorption sites) to the adsorbents is the main mechanism in the adsorption of CEX onto both the adsorbents [5].

**Table 3.** The film diffusion and intraparticle diffusion information of CEX adsorption onto NZVI.

| | | Film diffusion | | Intraparticle diffusion | | |
|---|---|---|---|---|---|---|
| Adsorbent | $C_0$ (mg/L) | $K_{fd}$ (min$^{-1}$) | $R^2$ | $K_{id}$ (mg/g-min$^{0.5}$) | C (mg/g) | $R^2$ |
| NNZVI | 25 | 0.118 | 0.999 | 42.38 | 13.21 | 0.920 |
| | 50 | 0.113 | 0.992 | 78.22 | 0.368 | 0.943 |
| | 100 | 0.118 | 0.991 | 136.47 | 2.24 | 0.947 |
| TNZVI | 25 | 0.070 | 0.996 | 33.05 | 7.68 | 0.891 |
| | 50 | 0.079 | 0.993 | 57.46 | 14.56 | 0.915 |
| | 100 | 0.086 | 0.991 | 104.43 | 38.67 | 0.940 |

Regarding that pseudo-first-order and pseudo-second-order kinetic models would not provide any information about the penetration mechanisms, and to assay whether mass transport (pore diffusion or intraparticle diffusion) takes place during the process, the intraparticle diffusion model, proposed by Weber and Morris [64] was examined. The mechanism of the penetration into the adsorbent can be determined using this model. The mathematical forms of the intraparticle diffusion model can be expressed by Equation (3):

$$q_t = K_{id} t^{0.5} + C, \tag{3}$$

where $K_{id}$ (mg/g min$^{1/2}$) and C (mg/g) are the constants of intraparticle diffusion. The latter parameter gives an indication of the thickness of the boundary layer. Another main step involved in the mass transfer of adsorbate is the liquid phase mass transport (or film diffusion) [65]. To understand whether adsorption of CEX onto NNZVI and TNZVI has been limited by film diffusion, the adsorption data from the experiments were also fitted to this model according to the following equation [51]:

$$\ln\left(1 - \frac{q_t}{q_e}\right) = -K_{fd} t, \tag{4}$$

where $K_{fd}$ (m$^{-1}$) is the liquid film diffusion constant. The data obtained from the fitting of the experimental data with intraparticle and film diffusion models for various initial CEX concentrations have been summarized in Table 3. The regression of $q_t$ versus $t^{1/2}$ for CEX was linear and did not pass through the origin, which shows that the boundary layer mass transfer controls the

**Table 2.** Adsorption kinetic parameters of CEX.

| | | Pseudo-first-order | | | | Pseudo-second-order | | | |
|---|---|---|---|---|---|---|---|---|---|
| Adsorbent | $C_0$(mg/L) | $k_1$(min$^{-1}$) | $q_e$(mg/g) | $R^2$ | $\chi^2$ | $k_2$(g/mg-min) | $q_e$ (mg/g) | $R^2$ | $\chi^2$ |
| NNZVI | 25 | 0.119 | 249.72 | 0.999 | 12.82 | 0.00042 | 304.54 | 0.994 | 58.59 |
| | 50 | 0.087 | 467.82 | 0.997 | 102.73 | 0.00014 | 602.46 | 0.988 | 357.81 |
| | 100 | 0.079 | 838.60 | 0.988 | 1080.80 | 0.00007 | 1098.45 | 0.980 | 1868.58 |
| TNZVI | 25 | 0.070 | 253.95 | 0.996 | 29.47 | 0.00019 | 319.97 | 0.990 | 83.85 |
| | 50 | 0.063 | 439.24 | 0.991 | 242.12 | 0.00011 | 551.51 | 0.978 | 576.87 |
| | 100 | 0.061 | 792.46 | 0.987 | 1133.66 | 0.00007 | 978.96 | 0.971 | 2514.95 |

adsorption process [51]. It is implied from the large values of C for all kinetic studies that the intraparticle diffusion was also involved in the adsorption process; however, this is not the only rate-limiting step [5]. It can also be seen that the $R^2$ values of the film diffusion model for adsorption of CEX onto NZVI at the experimental concentrations were higher than those of the intraparticle diffusion model. This finding suggests that diffusion through the boundary liquid layer around the adsorbent particles was the main controlling step [65]. Accordingly, a greater concentration gradient results in a higher rate of CEX molecules diffusing through the boundary layer surrounding the adsorbent, which, in turn, can cause a higher rate of adsorption.

### 3.3. Adsorption isotherms

The results expressed as plots of solid-phase CEX concentration versus liquid-phase CEX concentration have been shown in Figure 5. The parameters of the two isotherm models, applied in this study, and the calculated parameters for CEX adsorption onto the NNZVI and TNZVI have been given in Table 4. As shown in this table, based on $R^2$ and $\chi^2$ statistics, the adsorption of CEX onto the synthesized NNZVI is well described with the Freundlich isotherm model while in the case of TNZVI the Langmuir model was found to be the best. In the Langmuir model, it was assumed that there are homogeneous adsorbent surfaces with

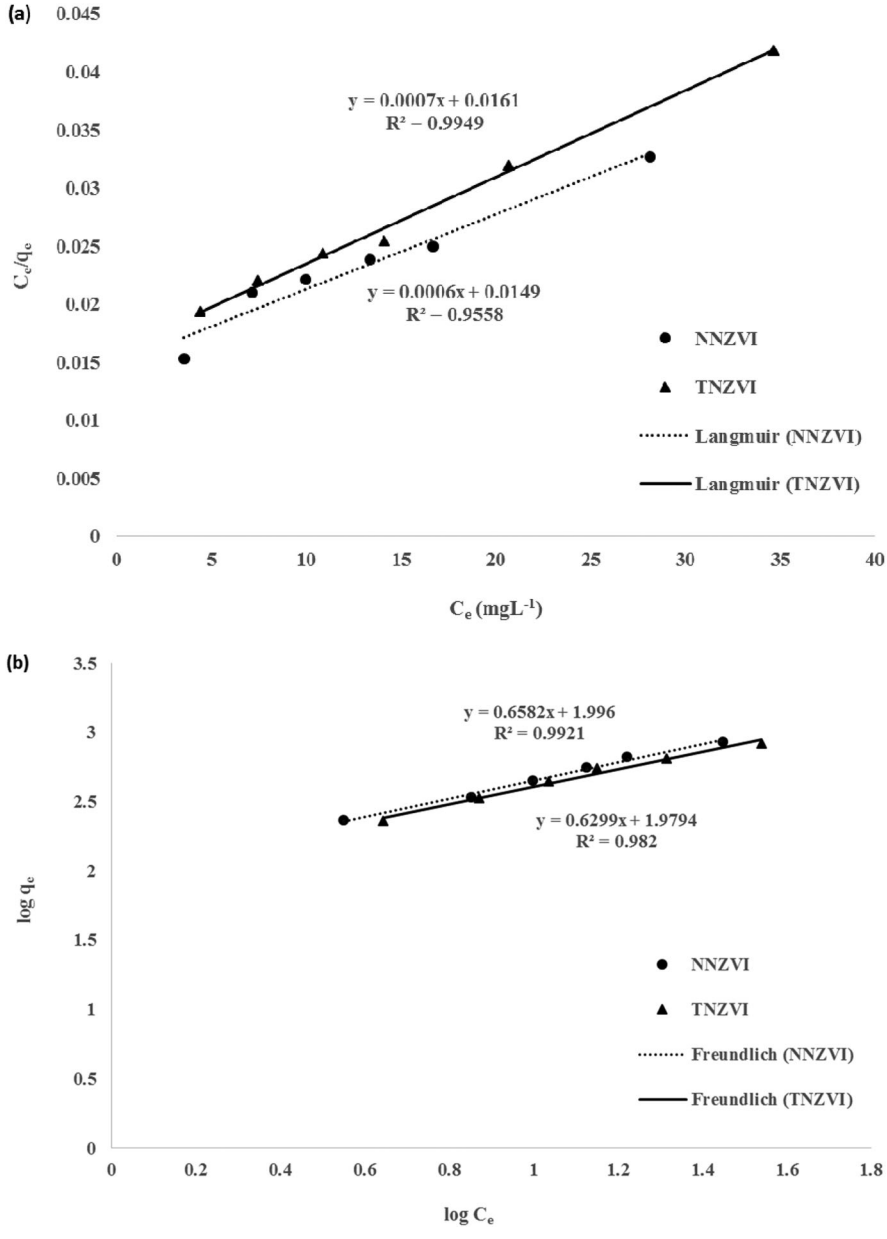


**Figure 5.** Experimental and predicted two-parameter isotherms of CEX according to the (a) Langmuir and (b) Freundlich models.

**Table 4.** Parameters of the Langmuir and Freundlich models for CEX adsorption onto NNZVI and TNZVI.

| | Adsorbent | |
|---|---|---|
| Isotherm models | NNZVI | TNZVI |
| Langmuir | | |
| $q_{max}$ (mg/g) | 1667 | 1428 |
| b (L/mg) | 0.0372 | 0.0032 |
| $R^2$ | 0.956 | 0.994 |
| $\chi^2$ | 19872.43 | 15842.08 |
| Freundlich | | |
| $K_f$ (mg/g) (mg/L)$^n$ | 99.08 | 95.36 |
| $n$ | 1.519 | 1.587 |
| $R^2$ | 0.992 | 0.982 |
| $\chi^2$ | 12871.33 | 38645.52 |

identical adsorption sites [66]. The Freundlich isotherm [67] is an empirical equation which assumes that the adsorption process takes place on a heterogeneous surface through a multilayer adsorption mechanism. The values of adsorption capacities ($q_m$) of NNZVI and TNZVI were found to be 1667 and 1428 mg/g, respectively, which were significantly high. Considering that CEX adsorption onto TNZVI follows the Langmuir assumption, it is reasonable to infer that the adsorption of CEX occurred in the form of mono-layer adsorption. Thus, both small sizes of NZVI and mono-layer behavior of prepared adsorbents have contributed to high CEX removal. The adsorbed CEX from the solution could be removed by following the sedimentation and separation steps [59].

The constant $n$ in the Freundlich equation is a constant that represents the parameter characterizing the quasi-gaussian energetic heterogeneity of the adsorption surface [68]. The $n$ constant gives an indication on the favorability of adsorption. It is generally stated that the values of $n$ in the range of 2–10 represent good, 1–2 moderately difficult and less than 1 poor adsorption characteristics [69]. The Freundlich exponent $1/n$ provides information on surface heterogeneity and surface affinity for the solute. This exponent was found to be 0.501 and 0.505 for NNZVI and TNZVI, respectively. These values indicate that the adsorption process is favorable.

To determine the characteristic of the adsorption process and to examine whether the adsorption is favorable in terms of $R_L$, a dimensionless constant, commonly known as separation factor, is calculated using Equation (5) [70]:

$$R_L = \frac{1}{(1 + bC_0)}. \quad (5)$$

The value of $R_L$ indicates the adsorption nature to be unfavorable ($R_L > 1$), linear ($R_L = 1$), favorable ($0 < R_L < 1$) or irreversible ($R_L = 0$). The value of $R_L$ obtained for CEX adsorption on NNZI was in the range of 0.12–0.86. Moreover, the $R_L$ values indicate favorable adsorption of CEX onto adsorbents as it lies between 0 and 1. The Langmuir constant $b$ was found to be 0.0372 for NNZVI and 0.0032 for TNZVI. These values also indicate a similar affinity of CEX for both adsorbents, which were expected.

### 3.4. Effect of solution pH on CEX adsorption

The pH of the solution is considered as one of the most important factors affecting the adsorption processes. Because of its immense importance, the CEX removal efficiency as a function of pH change was assessed for a series of initial pH values of 2, 4, 6, 7, 9 and 11 (Figure 6). The adsorption experiments for both adsorbents at each pH were carried out in triplicate and the average results have been presented in the figure. As shown, increasing initial solution pH value led to a decrease in removal efficiency. According to Figure 6, the percentage of CEX adsorption onto TNZVI decreased from 83.8% to 55.9% when the pH increased from 2 to 11. NNZVI has also shown the same trend (maximum CEX adsorption in acidic pH) but the minimum removal efficiency of 75.88% was observed at pH = 7. Thus, acidic conditions were favorable for CEX removal by NZVI compared to higher pH values. To explain the effects of solution pH on the CEX removal, both the surface charge of the adsorbents ($pH_{zpc}$) and the dissociation constant ($pK_a$) of CEX should be taken into account. This means that the variation in the pH of the solution results in the change of surface charge and the functional group chemistry of the adsorbents' surface [71]. Since the $pH_{pzc}$ of NNZVI and TNZVI were 4.4 and 5.6, respectively, (Figure 7), a positive charge developed on their surfaces at pH below $pH_{pzc}$. CEX is a zwitterionic molecule and a weak acid, thus although primarily dissociated as an acid ($pK_a = 5.2$), it has an amphoteric behavior and also has a $pK_a$ value of 2.56

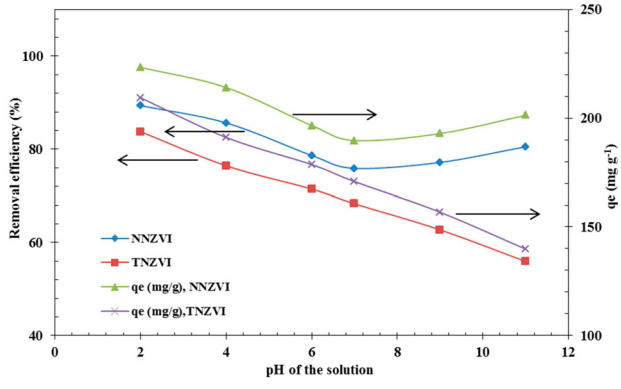


**Figure 6.** Effect of pH on CEX removal (initial concentration = 25 mg/L, optimum dose = 0.1 g/L and contact time = 20 min).

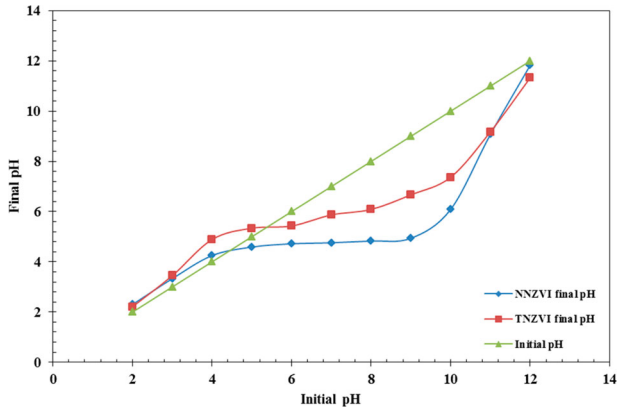


**Figure 7.** $pH_{zpc}$ of NNZVI and TNZVI.

and 6.88 [72,73]. Therefore, in an acidic solution (mainly $pH_s$ = 2–6), it shows cationic properties and exists as a zwitterion species, so dissociation of carboxylic group (–COOH) existing in the CEX molecule into carboxylate ($–COO^-$) occurred. Therefore, electrostatic attraction between the CEX (anionic) molecules (through $COO^-$ functional groups) and the positively charged surface of the adsorbents at the $pH_s$ below $pH_{zpc}$ (4.4 and 5.4 for NNZVI and TNZVI, respectively) was most probably the prevalent adsorption mechanism [51]. In the same way, the reduction of CEX adsorption at alkaline solution pH ($pH > pH_{pzc}$) resulted from the negative charge on the surface of the NZVI as well as occupying the adsorbent surfaces with $OH^-$ ions, which, in turn, leads to activate electrostatic repulsion of the adsorbate that has already been adsorbed on the adsorbent [5]. The increases of CEX adsorption by TNZVI beyond pH 7 (alkaline solution) could be explained by the dissociation of the protonated α-amino groups and catalytic degradation through intra molecular-nucleophilic attack of the side-chain alpha-amino group upon the beta-lactam carbonyls to produce diketopiperazine derivatives with the $NH_2^+$ functional group [74] which could easily be adsorbed by the negatively charged adsorbent surface. Moreover, some oppositely charged surface sites can still simultaneously exist on the adsorbent. The behavior of CEX sorption versus pH in this study is similar to those obtained by Legnoverde [75] who reported that the adsorption of CEX, at pH values around 2.3, was higher than that of pH range from 3 to 8.

### 3.5. Effect of adsorbent dosages on CEX adsorption

The effect of dosages of the synthesized adsorbent in the range of 0.01–0.25 g/L on the CEX removal by NNZVI and TNZVI was studied and the results are shown in Figure 8 respectively. As seen, the removal efficiencies and dosages of both the adsorbents have linear relationships. The removal efficiency of CEX was also increased with the increase of dosages but it has little impact in higher dosages; so, 0.1 g/L was selected as the optimum value for further study. This enhancement could be mainly due to increased available surface area for adsorption and reaction sites [76].

It can be concluded that the maximum adsorption capacity of CEX onto NNZVI and TNZVI obtained in this study is better than those displayed by other adsorbents that have been tested for the adsorption of CEX in the literature as seen in Table 5. From this observation, it may be suggested that CEX was favorably adsorbed onto the synthesized adsorbents. NNZVI and TNZVI can be considered as suitable and eco-friendly adsorbents owing to their high adsorption capacity towards CEX, the availability of their precursors (Nettle and Thyme) in abundance and low costs.

### 3.6. Removal mechanisms of CEX

The suggested pathways of NZVI for pollutants' removal include adsorption, complexation, enmeshment and

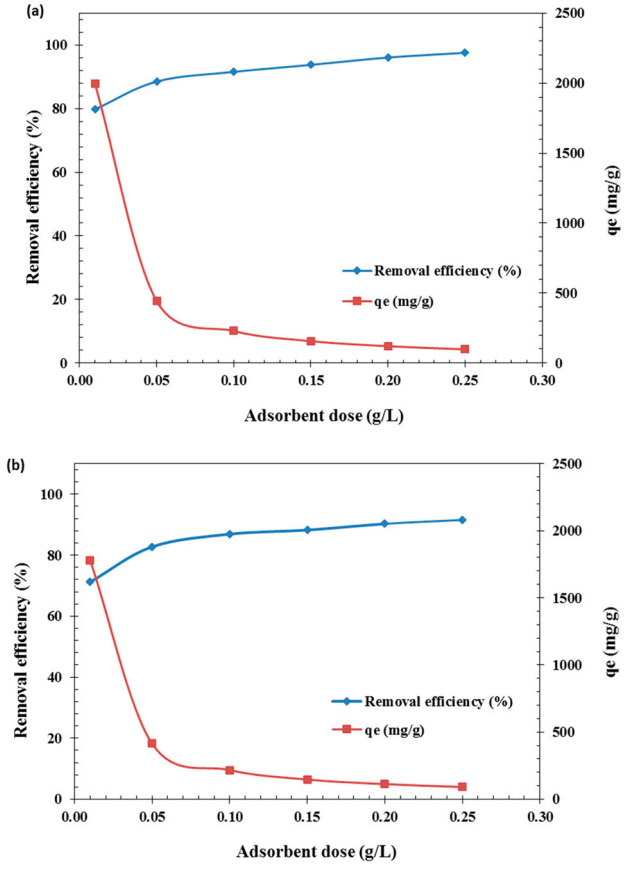


**Figure 8.** Effect of adsorbent dose on the adsorption of CEX by (a) NNZVI and (b) TNZVI (pH = 2, contact time = 20 min, shaking speed = 200 rpm at room temperature).

**Table 5.** Comparison of different pollutants' removal by iron nanoparticles and CEX removal by various adsorbents.

| Pollutant | Adsorbent | Isotherm parameters for adsorption | | Removal efficiency | Ref. |
|---|---|---|---|---|---|
| | | $q_{max}$ (mg/g) | $b$ (L/mg) | | |
| Antimony | NZVI | NA[a] | – | > 90% | [49] |
| Chloramphenicol | NZVI | NA[a] | – | ≈ 100 | [51] |
| Nitrate | NZVI | 13.06 | – | – | [34] |
| Arsenic (V) | NZVI | 94.67 | – | – | [44] |
| CEX | Activated carbon | 233.1 | 1.355 | – | [67] |
| CEX | Commercial–carbon | 222.3 | – | – | [68] |
| CEX | Cu–Activated carbon | 78.12 | 0.351 | – | [2] |
| CEX | NNZVI | 1667 | 0.0109 | ≈ 100 | Present study |
| CEX | TNZVI | 1428 | 0.0108 | ≈ 100 | Present study |

[a]not available.

coprecipitation as well as surface-mediated chemical reduction [77–79]. In the present work, the effluent was analyzed to determine the formation of any by-products using high-performance liquid chromatography (HPLC) (Shimadzu, LC10A HPLC) equipped with a UV detector (SPD-10AV). As seen in Figure 9(a, b), only one distinctive peak was observed (Figure 9(b)), revealing that CEX degradation did not occur. Therefore, it can be stated

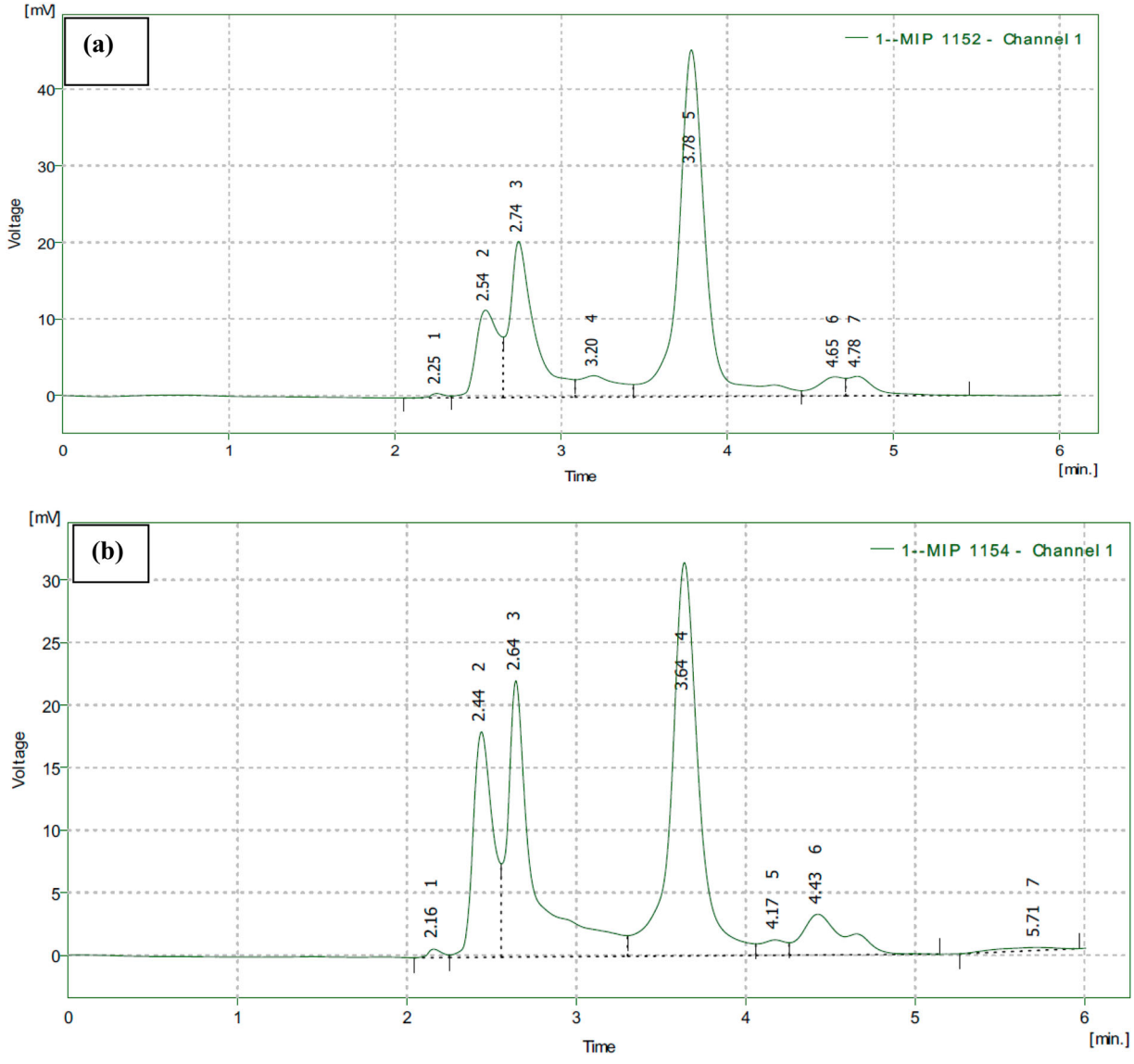


**Figure 9.** HPLC chromatogram of solution containing CEX (a) before and (b) after the adsorption process (initial concentration = 25 mg/L, pH = 2, contact time = 20 min, adsorbent dose = 0.1 g/L and shaking speed = 200 rpm at room temperature).

that the removal of CEX occurred mainly by the adsorption process and not by the reduction. These results are consistent with our previous study where Cr(VI) removal was reported by NZVI, synthesized from plant extracts [59]. Nevertheless, under the acidic condition (pH 2.0), corrosion rate of ZVI could be accelerated rapidly, and could generate some corrosion products (e.g. $Fe(OH)_2$/$Fe(OH)_3$) [78], which could also fairly absorb the pollutants and could play some role (although minor) in the CEX removal.

## 4. Conclusions

In this study, the adsorption of CEX onto novel synthesized nano-zero-valent irons (NZVI) from Nettle (NNZVI) and Thyme (TNZVI) leaf extracts via the green synthesis method was investigated. It was found that the CEX removal capacity of both these is significantly high. As the results showed, the monolayer adsorption capacities for CEX by NNZVI and TNZVI were found to be 1667 and 1428 mg/g, respectively. These values are comparable with the best commercially available activated carbons.

The adsorption kinetics of CEX on NNZVI and TNZVI could be explained by Lagergren's pseudo-first-order kinetic model. The optimum pH for the adsorption of CEX was found to be 2.0 and about two hours is needed to reach the equilibrium for both the adsorbents. Furthermore, HPLC results, under studied conditions, did not show any distinctive peaks for the degradation by-products, thus confirming that adsorption was the main removal mechanism in this study. Thus, considering the findings of this study, the developed nanoparticles from Nettle and Thyme leaf extracts, as low-cost adsorbents, have high potential for the removal of CEX from aqueous solution and these materials could be considered as promising adsorbents for antibiotics and probably other organic pollutants' removal from aqueous solutions.

## Acknowledgements

The authors would like to acknowledge Ardabil University of Medical Sciences for instrumental support.

## Disclosure statement

No potential conflict of interest was reported by the authors.

## Funding

This work was supported by the Ardabil University of Medical Sciences [Grant Number 9501].

## ORCID

*Mostafa Leili* http://orcid.org/0000-0001-6209-0038
*Mehdi Fazlzadeh* http://orcid.org/0000-0001-9512-6025
*Amit Bhatnagar* http://orcid.org/0000-0002-3565-9943

## References

[1] Gao J, Chen J, Li X, et al. Azide-functionalized hollow silica nanospheres for removal of antibiotics. J Colloid Interface Sci. 2015;444:38–41.
[2] Dargahi A, Pirsaheb M, Hazrati S, et al. Evaluating efficiency of H2O2 on removal of organic matter from drinking water. Desalination Water Treat. 2015;54:1589–1593.
[3] Liu H, Liu W, Zhang J, et al. Removal of cephalexin from aqueous solutions by original and Cu (II)/Fe (III) impregnated activated carbons developed from lotus stalks kinetics and equilibrium studies. J Hazard Mater. 2011;185:1528–1535.
[4] Fazlzadeh M, Ahmadfazeli A, Entezari A, et al. Removal of cephalexin using green montmorillonite loaded with $TiO_2$ nanoparticles in the presence potassium permanganate from aqueous solution. Koomesh. 2016;18:388–396.
[5] Samarghandi MR, Al-Musawi TJ, Mohseni-Bandpi A, et al. Adsorption of cephalexin from aqueous solution using natural zeolite and zeolite coated with manganese oxide nanoparticles. J Mol Liq. 2015;211:431–441.
[6] Pouretedal H, Sadegh N. Effective removal of amoxicillin, cephalexin, tetracycline and penicillin G from aqueous solutions using activated carbon nanoparticles prepared from vine wood. J Water Process Eng. 2014;1:64–73.
[7] Ji Y, Ferronato C, Salvador A, et al. Degradation of ciprofloxacin and sulfamethoxazole by ferrous-activated persulfate: implications for remediation of groundwater contaminated by antibiotics. Sci Total Environ. 2014;472:800–808.
[8] Liu W, Xie H, Zhang J, et al. Sorption removal of cephalexin by $HNO_3$ and $H_2O_2$ oxidized activated carbons. Sci China Chem. 2012;55:1959–1967.
[9] Ahmed MJ, Theydan SK. Adsorption of cephalexin onto activated carbons from *Albizia lebbeck* seed pods by microwave-induced KOH and $K_2CO_3$ activations. Chem Eng J. 2012;211–212:200–207.
[10] LaPara TM, Burch TR, McNamara PJ, et al. Tertiary-treated municipal wastewater is a significant point source of antibiotic resistance genes into Duluth-superior harbor. Environ Sci Technol. 2011;45:9543–9549.
[11] Fazlzadeh M, Rahmani A, Nasehinia HR, et al. Degradation of sulfathiazole antibiotics in aqueous solutions by using zero valent iron nanoparticles and hydrogen peroxide. Koomesh. 2016;18:350–356.
[12] Li Z, Hong H, Liao L, et al. A mechanistic study of ciprofloxacin removal by kaolinite. Colloids Surf B: Biointerfaces. 2011;88:339–344.
[13] Guo W, Wang H, Shi Y, et al. Sonochemical degradation of the antibiotic cephalexin in aqueous solution. Water Sa. 2010;36:651–654.
[14] Hadi M, Shokoohi R, Ebrahimzadeh Namvar A, et al. Antibiotic resistance of isolated bacteria from urban and hospital wastewaters in Hamadan City. Iran J Health Environ. 2011;4:105–114.

[15] Al-Gheethi AA, Norli I, Lalung J, et al. Biosorption of heavy metals and cephalexin from secondary effluents by tolerant bacteria. Clean Technol Environ Policy. 2014;16:137–148.
[16] Sundararaman S, Saravanane R. Effect of loading rate and HRT on the removal of cephalosporin and their intermediates during the operation of a membrane bioreactor treating pharmaceutical wastewater, (2010).
[17] Akhtar J, Amin NS, Junjie W. Optimization studies for catalytic ozonation of cephalexin antibiotic in a batch reactor. J Water Suppl: Res Technol—AQUA. 2012;61:413–426.
[18] Akhtar J, Amin NS, Zahoor MK. Optimizing removal of cod from water by catalytic ozonation of cephalexin using response surface methodology. J Chem Soc Pak. 2013;35:1249–1253.
[19] Jafari M, Aghamiri S. Evaluation of carbon nanotubes as solid-phase extraction sorbent for the removal of cephalexin from aqueous solution. Desalination Water Treat. 2011;28:55–58.
[20] Niu H, Cai Y, Shi Y, et al. Evaluation of carbon nanotubes as a solid-phase extraction adsorbent for the extraction of cephalosporins antibiotics, sulfonamides and phenolic compounds from aqueous solution. Anal Chim Acta. 2007;594:81–92.
[21] Hassani A, Torabian A, Rahimi K. Performance of iron-zero (nZVI) nanno particles in removal of cephalexin from synthetic wastewater. J Water Wastewater. 2014;25:85–92.
[22] Zazouli M, Ulbricht M, Nasseri S, et al. Effect of hydrophilic and hydrophobic organic matter on amoxicillin and cephalexin residuals rejection from water by nanofiltration. Iranian J Environ Health Sci Eng. 2010;7:15–24.
[23] Moussavi G, Yazdanbakhsh A, Heidarizad M. The removal of formaldehyde from concentrated synthetic wastewater using O3/MgO/H2O2 process integrated with the biological treatment. J Hazard Mater. 2009;171:907–913.
[24] Li K, Yediler A, Yang M, et al. Ozonation of oxytetracycline and toxicological assessment of its oxidation by-products. Chemosphere. 2008;72:473–478.
[25] Almasi A, Dargahi A, Amrane A, et al. Effect of the retention time and the phenol concentration on the stabilization pond efficiency in the treatment of oil refinery wastewater. Fresenius Environ Bull. 2014;23:2541–2548.
[26] Comninellis C, Kapalka A, Malato S, et al. Advanced oxidation processes for water treatment: advances and trends for R&D. J Chem Technol Biotechnol. 2008;83:769–776.
[27] Manual EG. Alternative disinfectants and oxidants. Washington, DC: Disinfectant Use in Water Treatment; 1999.
[28] Parastar S, Nasseri S, Borji SH, et al. Application of Ag-doped $TiO_2$ nanoparticle prepared by photodeposition method for nitrate photocatalytic removal from aqueous solutions. Desalination Water Treat. 2013;51:7137–7144.
[29] Rahmani AR, Shabanloo A, Fazlzadeh M, et al. Investigation of operational parameters influencing in treatment of dye from water by electro-Fenton process. Desalination Water Treat. 2016;57:24387–24394.
[30] Khosravi R, Fazlzadehdavil M, Barikbin B, et al. Electrodecolorization of reactive Red 198 from aqueous solutions using aluminum electrodes systems: modeling and optimization of operating parameters. Desalination Water Treat. 2015;54:3152–3160.
[31] Li S-z, Li X-y, Wang D-z. Membrane (RO-UF) filtration for antibiotic wastewater treatment and recovery of antibiotics. Sep Purif Technol. 2004;34:109–114.
[32] Pirsaheb M, Dargahi A, Hazrati S, et al. Removal of diazinon and 2,4-dichlorophenoxyacetic acid (2, 4-D) from aqueous solutions by granular-activated carbon. Desalination Water Treat. 2014;52:4350–4355.
[33] Abdoallahzadeh H, Alizadeh B, Khosravi R, et al. Efficiency of EDTA modified nanoclay in removal of humic acid from aquatic solutions. J Mazandaran Univ Med Sci. 2016;26:111–125.
[34] Khosravi R, Fazlzadehdavil M, Barikbin B, et al. Removal of hexavalent chromium from aqueous solution by granular and powdered *Peganum harmala*. Appl Surf Sci. 2014;292:670–677.
[35] Iram M, Guo C, Guan Y, et al. Adsorption and magnetic removal of neutral red dye from aqueous solution using Fe3O4 hollow nanospheres. J Hazard Mater. 2010;181:1039–1050.
[36] Noori Sepehr M, Mohebi S, Abdlollahi Vahed S, et al. Removal of tetracycline from synthetic solution by natural LECA. J Environ Health Eng. 2014;1:301–311.
[37] Al-Khalisy RS, Al-Haidary AMA, Al-Dujaili AH. Aqueous phase adsorption of cephalexin onto bentonite and activated carbon. Sep Sci Technol. 2010;45:1286–1294.
[38] Fakhri A, Adami S. Adsorption and thermodynamic study of cephalosporins antibiotics from aqueous solution onto MgO nanoparticles. J Taiwan Inst Chem Eng. 2014;45:1001–1006.
[39] Ananth S, Arumanayagam T, Vivek P, et al. Direct synthesis of natural dye mixed titanium dioxide nano particles by sol–gel method for dye sensitized solar cell applications. Optik-Int J Light Electron Opt. 2014;125:495–498.
[40] Wang S, Lu M, Zhou G, et al. Systematic investigations into SrSnO3 nanocrystals (I) synthesis by using combustion and coprecipitation methods. J Alloys Compd. 2007;432:265–268.
[41] Fazlzadeh M, Abdoallahzadeh H, Khosravi R, et al. Removal of acid black 1 from aqueous solutions using Fe3O4magnetic nanoparticles. J Mazandaran Univ Med Sci. 2016;26:174–186.
[42] Huang L, Weng X, Chen Z, et al. Green synthesis of iron nanoparticles by various tea extracts: comparative study of the reactivity. Spectrochim Acta A: Mol Biomol Spectrosc. 2014;130:295–301.
[43] Hoag GE, Collins JB, Holcomb JL, et al. Degradation of bromothymol blue by 'greener'nano-scale zero-valent iron synthesized using tea polyphenols. J Mater Chem. 2009;19:8671–8677.
[44] Machado S, Stawiński W, Slonina P, et al. Application of Green zero-valent iron nanoparticles to the remediation of soils contaminated with ibuprofen. Sci Total Environ. 2013;461-462:323–329.
[45] Wang T, Lin J, Chen Z, et al. Green synthesized iron nanoparticles by Green tea and eucalyptus leaves extracts used for removal of nitrate in aqueous solution. J Clean Prod. 2014;83:413–419.
[46] Machado S, Pacheco JG, Nouws HPA, et al. Characterization of Green zero-valent iron nanoparticles produced with tree leaf extracts. Sci Total Environ. 2015;533:76–81.

[47] Xiao J, Yue Q, Gao B, et al. Performance of activated carbon/nanoscale zero-valent iron for removal of trihalomethanes (THMs) at infinitesimal concentration in drinking water. Chem Eng J. 2014;253:63–72.
[48] Kalhori EM, Yetilmezsoy K, Uygur N, et al. Modeling of adsorption of toxic chromium on natural and surface modified lightweight expanded clay aggregate (LECA). Appl Surf Sci. 2013;287:428–442.
[49] Kennedy LJ, Vijaya JJ, Kayalvizhi K, et al. Adsorption of phenol from aqueous solutions using mesoporous carbon prepared by two-stage process. Chem Eng J. 2007;132:279–287.
[50] McKay G, Hadi M, Samadi MT, et al. Adsorption of reactive dye from aqueous solutions by compost. Desalination Water Treat. 2011;28:164–173.
[51] Moussavi G, Alahabadi A, Yaghmaeian K, et al. Preparation, characterization and adsorption potential of the NH4 Cl-induced activated carbon for the removal of amoxicillin antibiotic from water. Chem Eng J. 2013;217:119–128.
[52] Prasad KS, Gandhi P, Selvaraj K. Synthesis of green nano iron particles (GnIP) and their application in adsorptive removal of As (III) and As (V) from aqueous solution. Appl Surf Sci. 2014;317:1052–1059.
[53] Tongpoothorn W, Sriuttha M, Homchan P, et al. Preparation of activated carbon derived from *Jatropha curcas* fruit shell by simple thermo-chemical activation and characterization of their physico-chemical properties. Chem Eng Res Des. 2011;89:335–340.
[54] Foo K, Hameed B. Adsorption characteristics of industrial solid waste derived activated carbon prepared by microwave heating for methylene blue. Fuel Process Technol. 2012;99:103–109.
[55] Baes A, Bloom P. Diffuse reflectance and transmission Fourier transform infrared (DRIFT) spectroscopy of humic and fulvic acids. Soil Sci Soc Am J. 1989;53:695–700.
[56] Niemeyer J, Chen Y, Bollag J-M. Characterization of humic acids, composts, and peat by diffuse reflectance Fourier-transform infrared spectroscopy. Soil Sci Soc Am J. 1992;56:135–140.
[57] Dorjee P, Amarasiriwardena D, Xing B. Antimony adsorption by zero-valent iron nanoparticles (nZVI): Ion chromatography–inductively coupled plasma mass spectrometry (IC–ICP-MS) study. Microchem J. 2014;116:15–23.
[58] Leili M, Faradmal J, Kosravian F, et al. A comparison study on the removal of phenol from aqueous solution using organomodified bentonite and commercial activated carbon. Avicenna J Environ Health Eng. 2015;2:18–23.
[59] Fazlzadeh M, Rahmani K, Zarei A, et al. A novel Green synthesis of zero valent iron nanoparticles (NZVI) using three plant extracts and their efficient application for removal of Cr (VI) from aqueous solutions. Adv Powder Technol. 2017;28:122–130.
[60] Xia S, Gu Z, Zhang Z, et al. Removal of chloramphenicol from aqueous solution by nanoscale zero-valent iron particles. Chem Eng J. 2014;257:98–104.
[61] Weng X, Huang L, Chen Z, et al. Synthesis of iron-based nanoparticles by green tea extract and their degradation of malachite. Ind Crops Prod. 2013;51:342–347.
[62] Benguella B, Benaissa H. Cadmium removal from aqueous solutions by chitin: kinetic and equilibrium studies. Water Res. 2002;36:2463–2474.
[63] Mohanty K, Das D, Biswas M. Adsorption of phenol from aqueous solutions using activated carbons prepared from tectona grandis sawdust by ZnCl2 activation. Chem Eng J. 2005;115:121–131.
[64] Wu F-C, Tseng R-L, Juang R-S. Initial behavior of intraparticle diffusion model used in the description of adsorption kinetics. Chem Eng J. 2009;153:1–8.
[65] Nethaji S, Sivasamy A. Adsorptive removal of an acid dye by lignocellulosic waste biomass activated carbon: equilibrium and kinetic studies. Chemosphere. 2011;82:1367–1372.
[66] Langmuir I. The adsorption of gases on plane surfaces of glass, mica and platinum. J Am Chem Soc. 1918;40:1361–1403.
[67] Freundlich H. Over the adsorption in solution. J Phys Chem. 1906;57:1100–1107.
[68] Bansal RC, Goyal M. Activated carbon adsorption. Florida: CRC press; 2005.
[69] Treybal RE, Treybal Robert E. Mass-transfer operations. New York: McGraw-Hill; 1968.
[70] Weber TW, Chakravorti RK. Pore and solid diffusion models for fixed-bed adsorbers. AIChE J. 1974;20:228–238.
[71] Crini G, Peindy HN, Gimbert F, et al. Removal of C.I. Basic Green 4 (Malachite Green) from aqueous solutions by adsorption using cyclodextrin-based adsorbent: kinetic and equilibrium studies. Sep Purif Technol. 2007;53:97–110.
[72] Giacomino N, Cerra M, Gumiy D, et al. Pharmacokinetic-pharmacodynamic modeling of antibacterial activity of cephalexin on E. coli in presence of canine serum. Rev Med Vet (Toulouse). 2012;163:431–440.
[73] Vilt ME, Ho WSW. Supported liquid membranes with strip dispersion for the recovery of cephalexin. J Memb Sci. 2009;342:80–87.
[74] Yamana T, Tsuji A. Comparative stability of cephalosporins in aqueous solution: kinetics and mechanisms of degradation. J Pharm Sci. 1976;65:1563–1574.
[75] Legnoverde MS, Simonetti S, Basaldella EI. Influence of pH on cephalexin adsorption onto SBA-15 mesoporous silica: theoretical and experimental study. Appl Surf Sci. 2014;300:37–42.
[76] Tarlani Azar M, Leili M, Taherkhani F, et al. A comparative study for the removal of aniline from aqueous solutions using modified bentonite and activated carbon. Desalination Water Treat. 2016;57:24430–24443.
[77] Fang Z, Chen J, Qiu X, et al. Effective removal of antibiotic metronidazole from water by nanoscale zero-valent iron particles. Desalination. 2011;268:60–67.
[78] Lai B, Zhou Y, Qin H, et al. Pretreatment of wastewater from acrylonitrile–butadiene–styrene (ABS) resin manufacturing by microelectrolysis. Chem Eng J. 2012;179:1–7.
[79] Miehr R, Tratnyek PG, Bandstra JZ, et al. Diversity of contaminant reduction reactions by zerovalent iron: role of the reductate. Environ Sci Technol. 2004;38:139–147.